AGU PUBLICATIONS

Geophysical Research Letters

RESEARCH LETTER
10.1002/2017GL073669

Key Points:
- Atmospheric convection parameterization is important in ENSO predictions
- Improving mean state simulations (e.g., solving the double-ITCZ problem) is important for ENSO predictions

Supporting Information:
- Supporting Information S1

Correspondence to:
J. Zhu,
jieshun.zhu@noaa.gov

Citation:
Zhu, J., A. Kumar, W. Wang, Z.-Z. Hu, B. Huang, and M. A. Balmaseda (2017), Importance of convective parameterization in ENSO predictions, *Geophys. Res. Lett.*, *44*, 6334–6342, doi:10.1002/2017GL073669.

Received 30 MAR 2017
Accepted 21 APR 2017
Accepted article online 24 APR 2017
Published online 28 JUN 2017

Importance of convective parameterization in ENSO predictions

Jieshun Zhu[1,2], Arun Kumar[1], Wanqiu Wang[1], Zeng-Zhen Hu[1], Bohua Huang[3,4], and Magdalena A. Balmaseda[5]

[1]Climate Prediction Center, NOAA/NWS/NCEP, College Park, Maryland, USA, [2]Earth System Science Interdisciplinary Center, University of Maryland, College Park, Maryland, USA, [3]Center for Ocean-Land-Atmosphere Studies, George Mason University, Fairfax, Virginia, USA, [4]Department of Atmospheric, Oceanic, and Earth Sciences, College of Science, George Mason University, Fairfax, Virginia, USA, [5]European Centre for Medium-Range Weather Forecasts, Reading, UK

Abstract This letter explored the influence of atmospheric convection scheme on El Niño–Southern Oscillation (ENSO) predictions using a set of hindcast experiments. Specifically, a low-resolution version of the Climate Forecast System version 2 is used for 12 month hindcasts starting from each April during 1982–2011. The hindcast experiments are repeated with three atmospheric convection schemes. All three hindcasts apply the identical initialization with ocean initial conditions taken from the European Centre for Medium-Range Weather Forecasts and atmosphere/land initial states from the National Centers for Environmental Prediction. Assessments indicate a substantial sensitivity of the sea surface temperature prediction skill to the different convection schemes, particularly over the eastern tropical Pacific. For the Niño 3.4 index, the anomaly correlation skill can differ by 0.1–0.2 at lead times longer than 2 months. Long-term simulations are further conducted with the three convection schemes to understand the differences in prediction skill. By conducting heat budget analyses for the mixed-layer temperature anomalies, it is suggested that the convection scheme having the highest skill simulates stronger and more realistic coupled feedbacks related to ENSO. Particularly, the strength of the Ekman pumping feedback is better represented, which is traced to more realistic simulation of surface wind stress. Our results imply that improving the mean state simulations in coupled (ocean-atmosphere) general circulation model (e.g., ameliorating the Intertropical Convergence Zone simulation) might further improve our ENSO prediction capability.

1. Introduction

Since the initial attempts about 30 years ago [e.g., *Cane et al.*, 1986], the capability of dynamical models to predict the El Niño–Southern Oscillation (ENSO) has improved significantly [e.g., *Ji et al.*, 1994; *Kirtman et al.*, 1997; *Chen et al.*, 1995; *Zhang et al.*, 2003; *Jin et al.*, 2008; *Barnston et al.*, 2012; *Zhu et al.*, 2012, 2013a, 2015]. It has been demonstrated that, on average, the sea surface temperature (SST) variability in the tropical Pacific associated with ENSO can be successfully predicted several seasons ahead, as quantified by the statistics of some given metrics (e.g., anomaly correlation of the Niño 3.4 index). On occasions, however, our ENSO predictions can still have notable failures and the forecasts are not yet reliable [e.g., *Zhu et al.*, 2013b]. Therefore, continued efforts are required to further our understanding of the ENSO dynamics and improving its prediction capability.

This study is to explore the influence of atmospheric convection scheme on ENSO predictions. Previous studies [e.g., *Guilyardi et al.*, 2004] identified a dominant role of the atmospheric component in a coupled model in determining the El Niño characteristics (e.g., periodicity and amplitude), although the ocean-related feedback processes are also very important [e.g., *Zhang et al.*, 2015]. Among various atmospheric factors, the cumulus convection scheme was suggested as of particular importance for determining the characteristics of ENSO simulations. By modifying the parameterization of deep convection, *Wu et al.* [2007] and *Neale et al.* [2008] demonstrated ENSO simulation improvements in their coupled (ocean-atmosphere) general circulation model (CGCM), which were linked to the enhanced intraseasonal variability with their new scheme. *Watanabe et al.* [2011] and *Kim et al.* [2011], using two different CGCMs, reported high sensitivity of ENSO amplitude to the entrainment rate in their convection scheme.

Despite above studies and the demonstration of the importance of convection schemes in ENSO simulations, to our knowledge, there have been no systematic studies about the sensitivity of ENSO prediction skill to

cumulus convections except for a case study about the 1997/1998 El Niño event [*Vitart et al.*, 2003]. The reason for this gap may be the following: it is known that ENSO prediction skill in a CGCM relies on both initialization and the model capability in simulating ENSO. Since initialization plays a crucial role [e.g., *Zhu et al.*, 2012], the ENSO prediction skill might not be sensitive to cumulus convection at least for short lead times, even though the ENSO properties may be highly sensitive to them in longer simulations. For the predictions at longer lead times, however, this sensitivity may play an increasingly important role in guiding the model trajectory, and it might become easier to discern the influence of convective parameterization on ENSO prediction skill. In fact, the choice of convective scheme for model forecasts/simulations is not based solely on ENSO prediction skill but instead is the best scheme for simulating convection in general. It is possible that the scheme that does an overall better job of representing convection might not be the best choice for ENSO predictions.

In this letter, hindcast experiments are performed to explore the effect of atmospheric convection schemes on ENSO predictions. The convection influence is isolated by a set of predictions under the same initial conditions but with different convection schemes. The applied convection schemes include the Simplified Arakawa-Schubert (SAS) cumulus convection scheme [*Pan and Wu*, 1995], the Relaxed Arakawa-Schubert (RAS) scheme [*Moorthi and Suarez*, 1992, 1999], and the Simplified Arakawa-Schubert version 2 (SAS2) scheme [*Han and Pan*, 2011]. *Wang et al.* [2015] tested the three convection schemes in an uncoupled framework to explore how the Madden-Julian Oscillation (MJO)-related tropical convection was predicted in the context of differences in various SST analyses. The ocean analysis chosen for initialization is the one producing the best SST prediction skill among others following our previous practice [*Zhu et al.*, 2012]. The rest of the letter is arranged as follows. The next section describes the model, data sets, and the experimental design. Section 3 presents our analyses. A summary is given in section 4.

2. Model, Experiments, and Data Sets

The model used in this study is a variant of National Centers for Environmental Prediction (NCEP) Climate Forecast System version 2 (CFSv2) [*Saha et al.*, 2014] with lower horizontal resolutions in both atmospheric and oceanic components. To distinguish from the standard CFSv2 that is currently used for the operational seasonal-to-interannual prediction at NCEP, the low-resolution CFSv2 is referred to as CFSv2L. In CFSv2L, the atmospheric model is the NCEP Global Forecast System (GFS) with a horizontal resolution at T62 and 64 vertical levels in a hybrid sigma-pressure coordinate. The ocean model is the Geophysical Fluid Dynamics Laboratory Molecular Ocean Model version 4. It is configured with a horizontal grid of $1° \times 1°$ poleward of 30°S and 30°N and meridional resolution increasing gradually to 0.33° between 10°S and 10°N. Vertically, it has 40 levels (27 of them in the upper 400 m) at constant depths, with maximum depth of approximately 4.5 km. The atmospheric and oceanic components exchange surface fluxes (i.e., momentum, heat, and freshwater fluxes, as well as SSTs) every 60 min. CFSv2L has been used for studies about the MJO [*Zhu et al.*, 2017a] and seasonal predictability [*Zhu et al.*, 2017b].

Different from the standard configuration of CFSv2 [*Saha et al.*, 2014], which uses the 2007 version of the NCEP operational GFS, the atmospheric component of CFSv2L is the 2011 version of the NCEP GFS, but the model physics are configured as in *Saha et al.* [2014]. In addition to the SAS convection scheme [*Pan and Wu*, 1995] used in *Saha et al.* [2014], there are two additional built-in convection schemes in the 2011 version of GFS, that is, the RAS scheme [*Moorthi and Suarez*, 1992, 1999] and the SAS2 scheme [*Han and Pan*, 2011]. SAS2 has been used in the NCEP operational GFS since 2011.

In this study, the three convection parameterization schemes (i.e., SAS, RAS, and SAS2) are applied for a set of ENSO retrospective forecast experiments. The forecast experiments start each April for the period of 1982–2011 and last for 12 months. ENSO prediction starting from spring is challenging, because weather noise originating in spring can have a large impact on the accuracy of ENSO prediction in subsequent boreal winter [*Larson and Kirtman*, 2016]. For all experiments, the same initializations are applied. Particularly, the ocean initial conditions (OICs) take the ocean states of the ECMWF Ocean Reanalysis System 4 [*Balmaseda et al.*, 2013] on 1 April. For each OIC, four ensemble members are used that differ in their atmospheric/land initial conditions, which apply the states at 0000 UTC of the first 4 days in each April in the NCEP Climate Forecast System Reanalysis (CFSR) [*Saha et al.*, 2010]. The ENSO prediction skill for these forecast experiments is evaluated by comparing the predicted ensemble mean SST anomalies (SSTAs) with the verified SST from

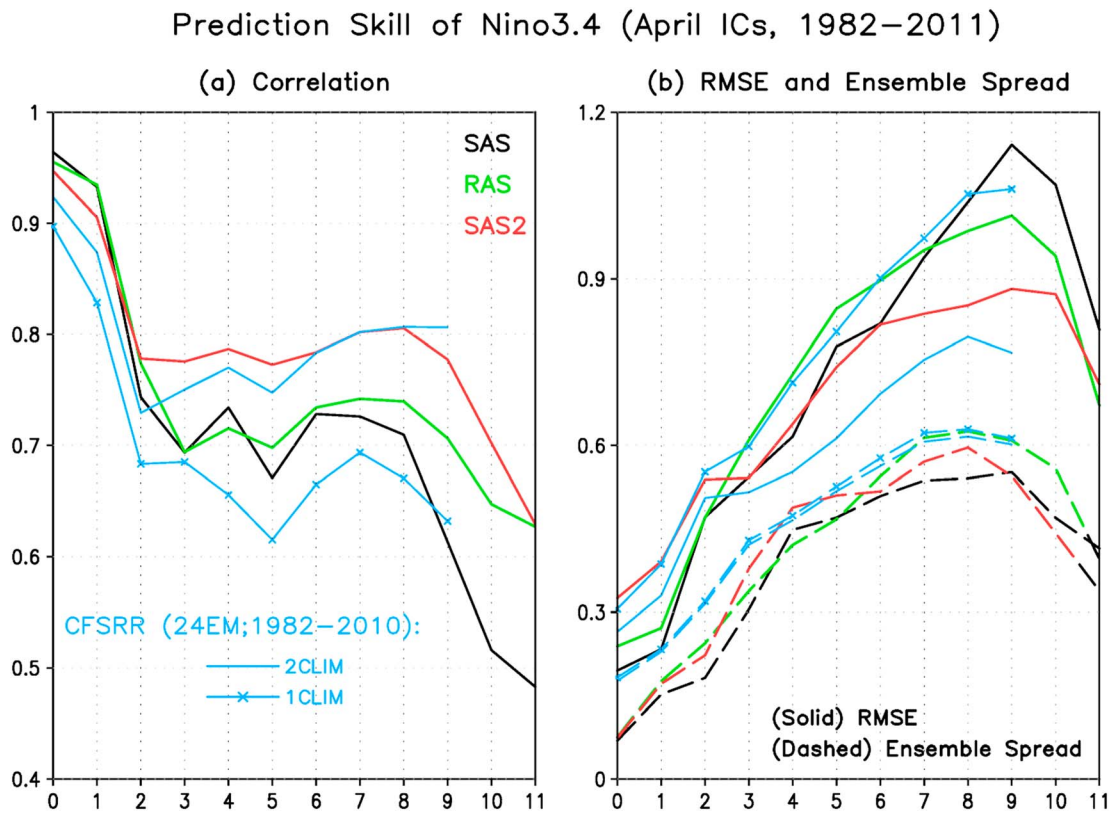

Figure 1. (a) Anomaly correlation coefficients and (b) RMSEs (°C) of Niño 3.4 index as a function of forecast lead months (*x* axis) for SAS (black), RAS (green), and SAS2 (red) convection schemes. The hindcasts start from the April initial conditions during 1982–2011. As a reference, the operational CFSv2 (i.e., CFSRR) skill shown in blue for the April starts during 1982–2010, with 24 ensemble members, and the curves with (without) X marks are for predictions with two climatologies (one climatology) applied for bias corrections.

OISST [*Reynolds et al.*, 2002]. The predicted SSTA is derived with respect to a lead time-dependent SST climatology, with no additional time smoothing applied. In this paper, the lead time is defined as follows: predictions for April (May) are defined as 0 month (1 month) lead.

In addition to the hindcast experiments, three coupled integrations (each lasting 68 years) are also conducted with each convection scheme, all starting from the ocean state of the NCEP Global Ocean Data Assimilation System (GODAS) [*Behringer*, 2005] and the atmosphere/land state of the CFSR [*Saha et al.*, 2010] on 1 January 1980. All analyses are based on the last 50 years by discarding the first 18 spin-up years. In addition to the verified SST from OISST [*Reynolds et al.*, 2002], other monthly data sets used for verifications include precipitation from the NOAA's CPC Merged Analysis of Precipitation (CMAP) [*Xie and Arkin*, 1997], wind stress from CFSR [*Saha et al.*, 2010], and subsurface ocean fields from GODAS [*Behringer*, 2005]. All climatological mean states are calculated for the period of 1982–2011.

3. Results

Figure 1 explored the prediction skill of Niño 3.4 SSTA time series by illustrating the anomaly correlation and root-mean-square error (RMSE) between the predicted and observed time series as a function of lead times. As a reference, the NCEP operational CFSv2 (i.e., CFSRR [*Saha et al.*, 2010]) skill is also shown. Measured by the anomaly correlation (Figure 1a), the three hindcasts exhibit comparable prediction skill at short lead times (i.e., at 0–2 lead months) when ENSO predictions are mostly influenced by the identical initial conditions among three hindcasts. We note that even if the convection parameterization has small or negligible impact on SST prediction at short lead times, it does not mean it is not important for these time scales [see *Vitart et al.*, 2007]. For lead times longer than 2 months, however, ENSO prediction skill exhibits a high sensitivity to convection schemes, with the anomaly correlation differences reaching 0.1 to 0.2. The hindcast with the

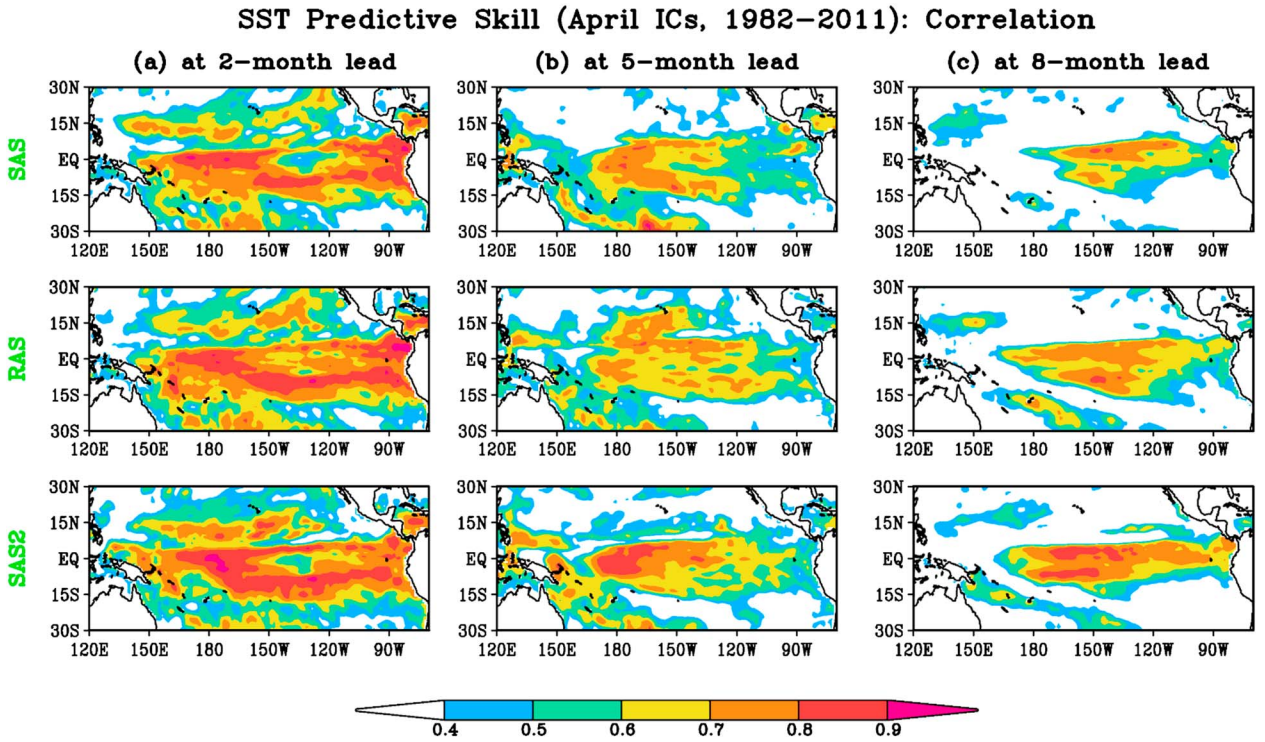

Figure 2. Distribution of anomaly correlations between observed and predicted SST anomalies at (a) 2, (b) 5, and (c) 8 month lead times in the first, second, and third columns, respectively. The upper, middle, and bottom rows are for forecasts with the SAS, RAS, and SAS2 convection schemes, respectively.

SAS2 is the best among the three, and its anomaly correlation skill is well above 0.75 (0.6) at all lead times shorter than 10 months (up to 12 months). In contrast, the hindcasts with RAS and SAS have the anomaly correlation skill of less than 0.75 at all lead times longer than 2 months. Between RAS and SAS, the correlation skill is generally comparable at lead times shorter than 9 months, but SAS has clearly lower skill at longer lead times with its anomaly correlation skill as low as 0.48 at the 11 month lead.

A comparison of RMSE (solid curves in Figure 1b) generally gives similar conclusions. For example, the RMSE exhibits the largest difference among the three hindcasts at long lead times, and SAS2 is generally the most skillful. Particularly, at the lead times of 7–10 months, while the SAS2 hindcast has RMSEs lower than 0.9°C, for the SAS hindcast, it could be as high as 1.14°C and the RAS hindcast generally lies in between. The better prediction of Niño 3.4 with SAS2 can actually be seen in the indices themselves. For instance, at the 8 month lead (corresponding to December; see Figure S1 in the supporting information), SAS2 tends to predict the correct phase of ENSO more often than SAS and RAS (i.e., fewer dots in quadrants 2 and 4). In terms of forecast reliability, hindcasts with the three convection schemes present generally comparable ensemble spreads (dashed curves in Figure 1b), all smaller than their RMSEs as in other systems [e.g., *Zhu et al.*, 2013b]. In addition, compared to the NCEP operational CFSv2 predictions (no matter whether one or two climatologies are applied for its bias corrections [*Xue et al.*, 2013]; blue curves in Figure 1), SAS2 has a comparable or even slightly better skill at some leads. This result is encouraging, considering that our experimental hindcasts have a much smaller ensemble size (4 versus 24) and lower resolutions (T62 versus T126 for atmosphere and 1° × 1° versus 0.5° × 0.5° for ocean).

Figure 2 presents the spatial distributions of SST prediction skill at the lead times of 2, 5, and 8 months. As expected, high skill is generally shown in the central and eastern tropical Pacific, where the seasonal SST variations are dominated by ENSO-related processes. At 2 month lead time (Figure 2a), consistent with Figure 1a, comparable and high SST prediction skill is achieved by three convection schemes and anomaly correlation is greater than 0.7 in most equatorial Pacific. As the lead time increases, the correlation skill drops quickly in the eastern tropical Pacific, and the skill difference also becomes more evident. At the 5 month lead (Figure 2b), for example, while anomaly correlation remains >0.6 over a sizable region of the central Pacific in three

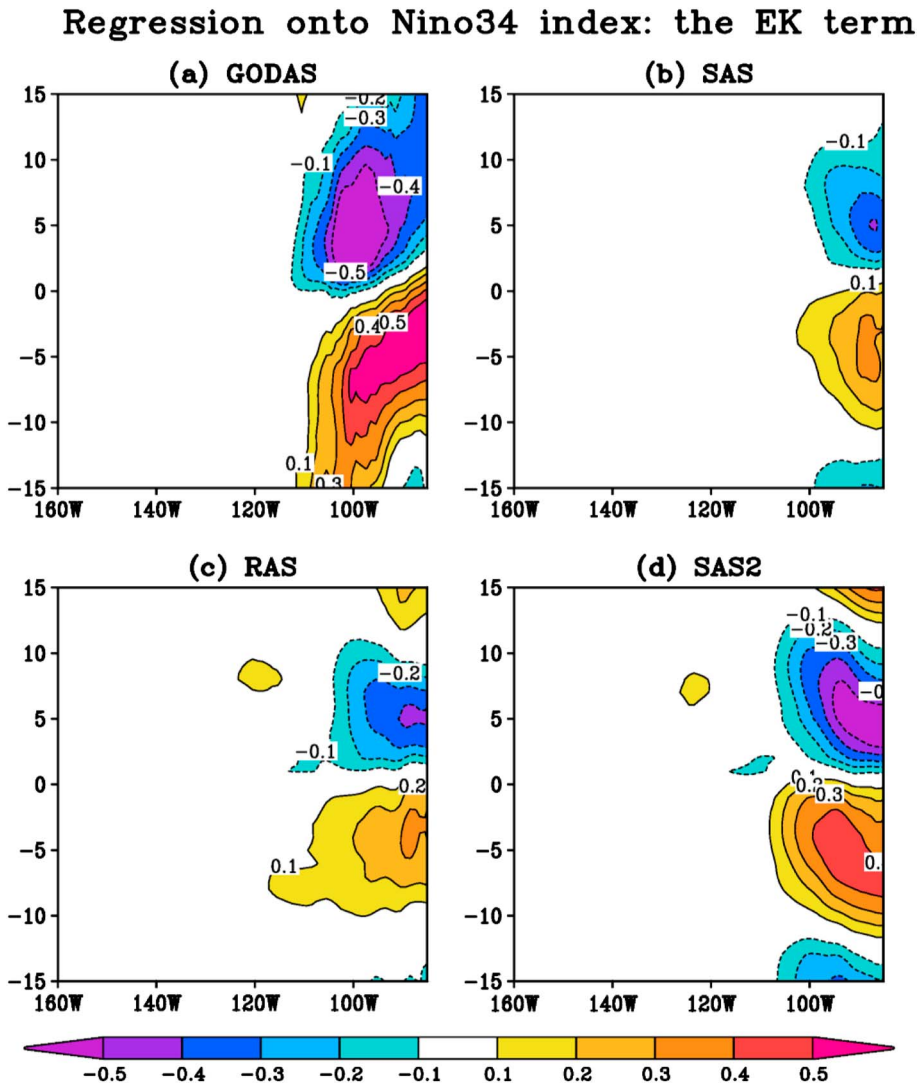

Figure 3. Longitude-time lag section of the Ekman pumping feedback term (EK) regressed onto Niño 3.4 index, in (a) GODAS and coupled simulations with (b) SAS, (c) RAS, and (d) SAS2 convection schemes. Units are month^{-1}. The *y* axis is the lag time in months.

hindcasts, it falls to <0.6 or ~0.6 in the east (particularly in the SAS hindcast). The superiority of SAS2 over SAS and RAS could be seen over the whole basin. In the western and central Pacific, while in SAS2 there is a sizable region with correlation skill above 0.8, SAS and RAS only reach 0.7. Also, in the eastern Pacific, while the skill with SAS is only around 0.5, with SAS2 it is around 0.6 and RAS lies in between. At the 8 month lead time (Figure 2c), for all three hindcasts, even though the skillful region becomes smaller, the correlation skill increases slightly in the central and eastern tropical Pacific, compared to that at the 5 month lead (Figure 2b). This skill rebound likely reflects the fact that the mature ENSO stage is generally easier to predict by models than its developing stage (the 8 month lead time corresponds to December, usually the ENSO peak season). This feature is also apparent in Figure 1a. On the other hand, the skill difference among three hindcasts is generally maintained for all lead times (Figure 2c), with SAS2 (SAS) showing the highest (lowest) skill and RAS lying in between.

The above skill comparisons suggest that ENSO prediction skill in a CGCM could be sensitive to different atmospheric convection schemes, and further, the differences are easier to discern at longer lead times. The differences in prediction skill are likely modulated by differences in the characteristics of ENSO variability in CGCM simulations with different convection schemes. To further validate the hypothesis and understand

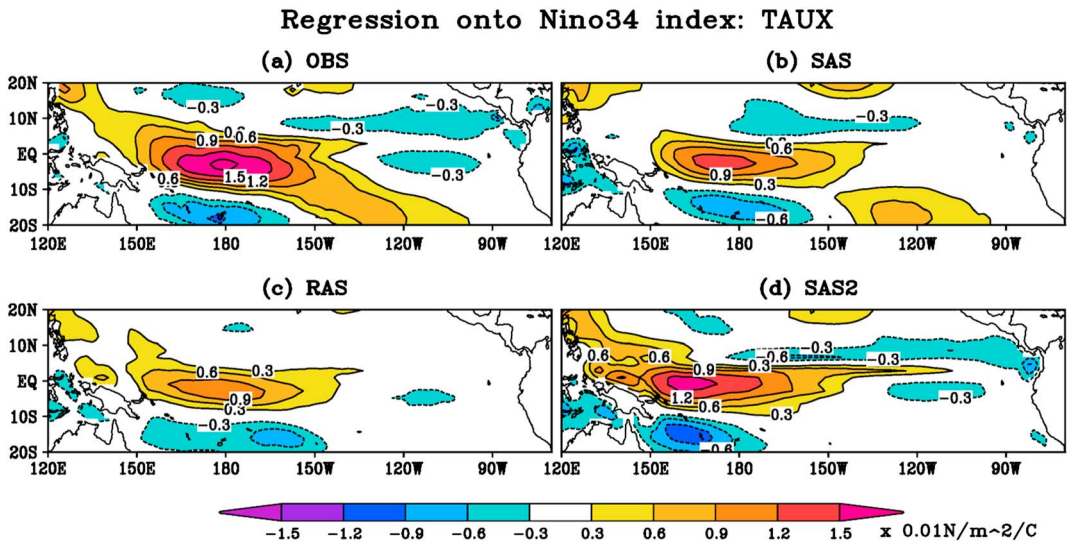

Figure 4. Regression of surface zonal wind stress anomalies onto Niño 3.4 index in (a) observations (OI SST and CFSR winds) and coupled simulations with the (b) SAS, (c) RAS, and (d) SAS2 convection schemes. Units are 0.01 $N/m^2/°C$.

the skill difference, coupled integrations are performed with the three convection schemes. A preliminary analysis suggests that CFSv2L with the three convection schemes presents some common biases in representing the ENSO features, e.g., a too regular and dominant 2 year period (see Figure S2) and a too strong amplitude (Figure S3). In comparison, RAS exhibits slightly more realistic ENSO periodicity than SAS and SAS2 (Figure S2). This is consistent with previous suggestions that ENSO simulations could be improved by a better representation of stochastic forcing [*Wu et al.*, 2007; *Neale et al.*, 2008], considering that the MJO is better simulated by RAS [*Zhu et al.*, 2017a]. The factor, however, might not be the critical one for the ENSO period bias in CFSv2L, in contrast to *Wu et al.* [2007] and *Neale et al.* [2008]. Instead, the meridionally too narrow structure and westward shift of zonal wind stress anomalies in the western Pacific (Figure 4) might be the dominant reasons shaping the ENSO period bias [*Kirtman*, 1997; *An and Wang*, 2000], which is not corrected by all three convection schemes.

To quantify differences in simulated ENSOs by the three convection schemes, heat budget analyses of mixed layer temperature anomalies are done for all simulations and the GODAS [*Behringer*, 2005]. A more detailed discussion of the methodology can be found in the supporting information [*Bjerknes*, 1969; *Suarez and Schopf*, 1988; *Battisti and Hirst*, 1989; *Picaut et al.*, 1996; *Jin*, 1997; *Kang et al.*, 2001; *Jin et al.*, 2003; *An and Jin*, 2004; *Behringer*, 2005; *Zhu et al.*, 2011]. Among various feedback terms, the zonal advective feedback, the Ekman pumping feedback (EK), the mean current effect (MA), and the thermocline feedback (TH) have been recognized as important factors for ENSO evolutions [e.g., *Bjerknes*, 1969; *Suarez and Schopf*, 1988; *Battisti and Hirst*, 1989; *Jin*, 1997; *Kang et al.*, 2001; *Picaut et al.*, 1996]. By comparing the terms among three simulations, it is found that they are all stronger and generally closer to GODAS in the SAS2 simulation than in the SAS and RAS simulations (see Figure S4).

Among the four feedback terms, the largest difference seems to occur in the amplitude of EK term in addition to its propagation (Figure 3). Specifically, in the SAS2 simulation (Figure 3a), prior to the peak phase of an El Niño, the EK term is as strong as 0.4 $month^{-1}$, and after that the EK term is around -0.5 $month^{-1}$. The amplitudes are comparable to those in GODAS (Figure 3d). In contrast, in the simulations with SAS (Figure 3b) or RAS (Figure 3c), the EK term is significantly smaller (by around 40%). In fact, because of the improvement in the EK term, the spatial structure of the SST anomalies is also improved (Figure S3). Thus, SAS2 is the only scheme which generates the maximum SST variability in the far eastern Pacific (Figure S3d) with a narrow meridional structure, in agreement with the observations (i.e., OISST; Figure S3a). In contrast, the other convection schemes produce peak in amplitude variability detached from the South American coast with wider meridional structure than observations (Figures S3b and S3c). The SST variance of the free running model is overall too strong in all the three simulations.

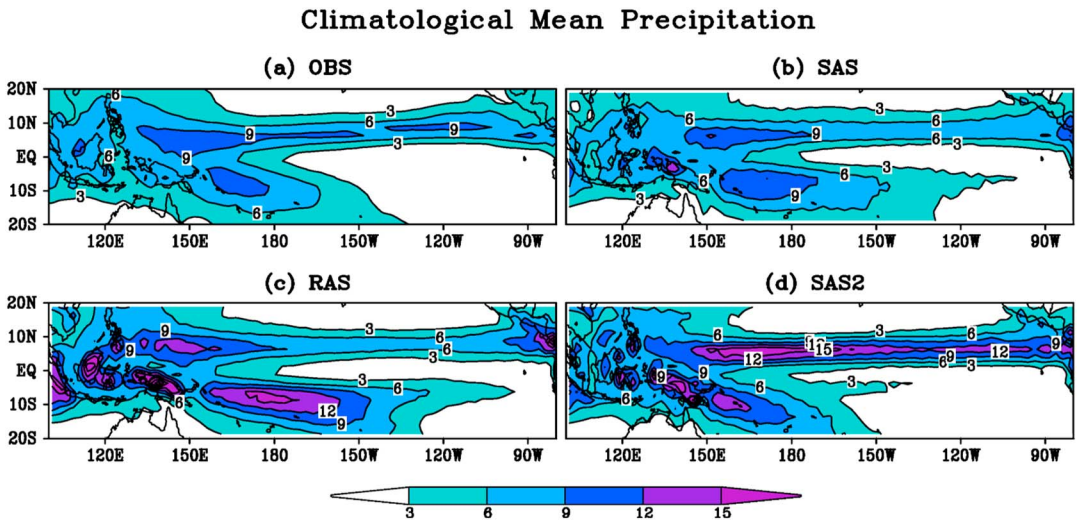

Figure 5. Climatological mean precipitations in (a) observations (CMAP) and coupled simulations with the (b) SAS, (c) RAS, and (d) SAS2 convection schemes. Units are mm/d.

The difference in the EK feedback term (Figure 3) is related to the difference in the surface zonal wind associated with ENSO in the eastern Pacific (Figure 4). Even though similar surface wind biases are present in the western Pacific for all three convection schemes (i.e., the too narrow meridional structure and westward shift of the maximal zonal wind anomalies), the regression pattern of the surface wind stress to Nino 3.4 exhibits clear improvements in the eastern Pacific with the SAS2 (Figure 4d). In particular, there are two bands of easterly wind stress anomalies (along around 9°N and 3°S) in the eastern Pacific stronger than 0.003 N/m^2 in association with the Niño 3.4 index of 1°C in the SAS2 simulation (Figure 4d). The feature is spatially coincident with that in observations (Figure 4a). In contrast, the easterly winds are far too weak for simulations with SAS and RAS (Figures 4b and 4c). Consequently, the variations of the local Ekman pumping could be much more realistic in the SAS2 simulation than in the SAS and RAS simulations (generally too weak in the latter two) and can explain for the difference in the EK feedback term among three simulations (Figure 3).

The improvement in ENSO feedback terms with SAS2 (Figure S4) might be associated with its better-simulated climatological precipitation distributions (Figure 5). Similar to most CGCMs, the simulations with SAS and RAS exhibit a double-ITCZ pattern (Figures 5b and 5c), in which the South Pacific Convergence Zone extends far too eastward. In the SAS2 simulation, in contrast, the climatological precipitation distribution, lacking the double-ITCZ feature, is clearly more realistic (Figure 5d), even though excessive precipitation still occurs over the whole tropics. It is noted that in these experiments the annual mean meridional asymmetry of precipitation in the tropical eastern Pacific is well correlated with that in SST and the equatorial meridional wind (Figure S5), consistent with the finding of *De Szoeke and Xie* [2008]. The more realistic precipitation distribution with SAS2 (Figure 5d) might explain the reason for more realistic zonal surface wind variability in the eastern Pacific (Figure 4d), which is likely related to the climatological ITCZ position, resulting in a more realistic EK term in the SAS2 simulation (Figure 3). In addition, in association with the improvement in precipitation distributions, the bias of too weak easterlies near the equator in both SAS and RAS simulations is clearly improved in the SAS2 simulation (Figure S6), which could contribute to enhancements in the MA and TH terms (Figures S4a and S4d) by modulating the climatological ocean currents.

4. Summary and Conclusions

Hindcast experiments are conducted in this study to explore the importance of atmospheric convection in ENSO prediction. Specifically, three atmospheric convection schemes (i.e., SAS, RAS, and SAS2) are applied in CFSv2L for 12 month hindcasts starting from each April during 1982–2011. Skill assessments identify substantial skill sensitivity in ENSO predictions associated with the three convection schemes. Particularly for the Niño 3.4 index, the anomaly correlation skill with SAS2 can be 0.1–0.2 higher than that with SAS at lead times longer than 2 months, and the skill with RAS generally lies in between. Further, coupled integrations are

conducted with the three convection schemes to explain the skill differences. Diagnostics suggest that, while the three convection schemes generate similar ENSO simulation biases (i.e., a too regular and dominant 2 year period and a too strong amplitude), SAS2 generally better represents the feedback terms important for ENSO evolution, particularly in the Ekman pumping feedback term. Specifically, compared with SAS and RAS, the SAS2 convection scheme can realistically represent the strength of the Ekman pumping feedback, which is responsible for a realistic distribution of SST anomalies in the far eastern Pacific. Furthermore, the Ekman process improvement is found related to the improvement in surface zonal winds in the eastern Pacific associated with ENSO, which are too weak in association with ENSO in the SAS and RAS simulations.

Lastly, the improvement in ENSO feedback terms seems to be associated with the simulation of climatological precipitation distributions. Specifically, the more realistic simulation of surface winds with SAS2 is arguably due to the improvement related to the double-ITCZ problem. Therefore, our results suggest that improving the mean state simulations in CGCMs (e.g., solving the double-ITCZ problem) might be an efficient way to further improve our ENSO prediction capability.

Acknowledgments
This study is supported by NOAA's Climate Program Office and Climate Observation Division. B.H. is supported by grants from NSF (AGS-1338427), NOAA (NA14OAR4310160), and NASA (NNX14AM19G). All data used in the paper are generated from sources expressed in the respective references.

References

An, S.-I., and F.-F. Jin (2004), Nonlinearity and asymmetry of ENSO, *J. Clim.*, *17*, 2399–2412.
An, S.-I., and B. Wang (2000), Interdecadal change of the structure of the ENSO mode and its impact on the ENSO frequency, *J. Clim.*, *13*, 2044–2055.
Balmaseda, M., K. Mogensen, and A. Weaver (2013), Evaluation of the ECMWF ocean reanalysis ORAS4, *Q. J. R. Meteorol. Soc.*, *139*, 1132–1161.
Barnston, A. G., M. K. Tippett, M. L. L'Heureux, S. Li, and D. G. DeWitt (2012), Skill of real-time seasonal ENSO model predictions during 2002–11: Is our capability increasing?, *Bull. Am. Meteorol. Soc.*, *93*, 631–651.
Battisti, D. S., and A. C. Hirst (1989), Interannual variability in the tropical atmosphere-ocean model: Influence of the basic state, ocean geometry and nonlineary, *J. Atmos. Sci.*, *45*, 1687–1712.
Behringer, D. W. (2005), The Global Ocean Data Assimilation System (GODAS) at NCEP, 11th Symposium on Integrated Observing and Assimilation Systems for the Atmosphere, Oceans, and Land Surface (IOAS-AOLS), San Antonio, TX, Amer. Meteor. Soc., 3.3.
Bjerknes, J. (1969), Atmospheric teleconnections from the equatorial Pacific, *Mon. Weather Rev.*, *97*, 163–172.
Cane, M. A., S. E. Zebiak, and S. C. Dolan (1986), Experimental forecast of El Niño, *Nature*, *321*, 827–832.
Chen, D., S. E. Zebiak, A. J. Busalacchi, and M. A. Cane (1995), An improved procedure for El Niño forecasting: Implications for predictability, *Science*, *269*, 1699–1702.
De Szoeke, S. P., and S. P. Xie (2008), The tropical eastern Pacific seasonal cycle: Assessment of errors and mechanisms in IPCC AR4 coupled ocean-atmosphere general circulation models, *J. Clim.*, *21*, 2573–2590.
Guilyardi, E., et al. (2004), Representing El Niño in coupled ocean-atmosphere GCMs: The dominant role of the atmospheric component, *J. Clim.*, *17*, 4623–4629, doi:10.1175/JCLI-3260.1.
Han, J., and H. L. Pan (2011), Revision of convection and vertical diffusion schemes in the NCEP Global Forecast System, *Weather Forecasting*, *26*, 520–533, doi:10.1175/WAF-D-10-05038.1.
Ji, M., A. Kumar, and A. Leetmaa (1994), An experimental coupled forecast system at the National Meteorological Center: Some early results, *Tellus, Ser. A*, *46*, 398–418.
Jin, E. K., et al. (2008), Current status of ENSO prediction skill in coupled ocean-atmosphere models, *Clim. Dyn.*, *31*, 647–664.
Jin, F.-F. (1997), An equatorial ocean recharge paradigm for ENSO. Part I: Conceptual model, *J. Atmos. Sci.*, *54*, 811–829.
Jin, F.-F., S.-I. An, A. Timmermann, and J. Zhao (2003), Strong El Niño events and nonlinear dynamical heating, *Geophys. Res. Lett.*, *30*(3), 1120, doi:10.1029/2002GL016356.
Kang, I.-S., S.-I. An, and F.-F. Jin (2001), A systematic approximation of the SST anomaly equation for ENSO, *J. Meteorol. Soc. Jpn.*, *79*, 1–10.
Kim, D., Y.-S. Jang, D.-H. Kim, Y.-H. Kim, M. Watanabe, F.-F. Jin, and J.-S. Kug (2011), El Niño–Southern Oscillation sensitivity to cumulus entrainment in a coupled general circulation model, *J. Geophys. Res.*, *116*, D22112, doi:10.1029/2011JD016526.
Kirtman, B. P. (1997), Oceanic Rossby wave dynamics and the ENSO period in a coupled model, *J. Clim.*, *10*, 1690–1704.
Kirtman, B. P., J. Shukla, B. Huang, Z. Zhu, and E. K. Schneider (1997), Multi-seasonal predictions with a coupled tropical ocean global atmosphere system, *Mon. Weather Rev.*, *125*, 789–808.
Larson, S. M., and B. P. Kirtman (2016), Drivers of coupled model ENSO error growth dynamics and the spring predictability barrier, *Clim. Dyn.*, doi:10.1007/s00382-016-3290-5.
Moorthi, S., and M. J. Suarez (1992), Relaxed Arakawa-Schubert: A parameterization of moist convection for general circulation models, *Mon. Weather Rev.*, *120*, 978–1002.
Moorthi, S., and M. J. Suarez (1999), Documentation of version 2 of Relaxed Arakawa-Schubert cumulus parameterization with convective downdrafts, NOAA Office Note 99–01, 44 pp.
Neale, R. B., J. H. Richter, and M. Jochum (2008), The impact of convection on ENSO: From a delayed oscillator to a series of events, *J. Clim.*, *21*, 5904–5924.
Pan, H.-L., and W.-S. Wu (1995), Implementing a mass flux convection parameterization package for the NMC Medium-Range Forecast Model, NMC Office Note 409, 39 pp.
Picaut, J., M. Ioualalen, C. Menkes, T. Delcroix, and M. McPhaden (1996), Mechanism of the zonal displacements of the Pacific warm pool, implications for ENSO, *Science*, *274*, 1486–1489.
Reynolds, R. W., N. A. Rayner, T. M. Smith, D. C. Stokes, and W. Q. Wang (2002), An improved in situ and satellite SST analysis for climate, *J. Clim.*, *15*, 1609–1625.
Saha, S., et al. (2010), The NCEP Climate Forecast System Reanalysis, *Bull. Am. Meteorol. Soc.*, *91*, 1015–1057.
Saha, S., et al. (2014), The NCEP Climate Forecast System version 2, *J. Clim.*, *27*, 2185–2208.
Suarez, M. J., and P. S. Schopf (1988), A delayed action oscillator for ENSO, *J. Atmos. Sci.*, *45*, 3283–3287.
Vitart, F., M. A. Balmaseda, L. Ferranti, and D. Anderson (2003), Westerly wind events and the 1997/98 El Niño event in the ECMWF seasonal forecasting system, *J. Clim.*, *16*, 3153–3170.

Vitart, F., S. Woolnough, M. A. Balmaseda, and A. Tompkins (2007), Monthly forecast of the Madden-Julian oscillation using a coupled GCM, *Mon. Weather Rev.*, *135*, 2700–2715, doi:10.1175/MWR3415.1.

Wang, W., A. Kumar, J. X. Fu, and M.-P. Hung (2015), What is the role of the sea surface temperature uncertainty in the prediction of tropical convection associated with the MJO?, *Mon. Weather Rev.*, *143*, 3156–3175.

Watanabe, M., M. Chikira, Y. Imada, and M. Kimoto (2011), Convective control of ENSO simulated in MIROC, *J. Clim.*, *24*, 543–562.

Wu, X., L. Deng, X. Song, G. Vettoretti, W. R. Peltier, and G. J. Zhang (2007), Impact of a modified convective scheme on the MJO and ENSO in a coupled climate model, *Geophys. Res. Lett.*, *34*, L16823, doi:10.1029/2007GL030637.

Xie, P., and P. A. Arkin (1997), Global precipitation: A 17-year monthly analysis based on gauge observations, satellite estimates, and numerical model outputs, *Bull. Am. Meteorol. Soc.*, *78*, 2539–2558.

Xue, Y., M. Chen, A. Kumar, Z.-Z. Hu, and W. Wang (2013), Prediction skill and bias of tropical Pacific sea surface temperatures in the NCEP Climate Forecast System version 2, *J. Clim.*, *26*, 5358–5378, doi:10.1175/JCLI-D-12-00600.1.

Zhang, R.-H., S. E. Zebiak, R. Kleeman, and N. Keenlyside (2003), A new intermediate coupled model for El Niño simulation and prediction, *Geophys. Res. Lett.*, *30*(19), 2012, doi:10.1029/2003GL018010.

Zhang, R.-H., C. Gao, X. Kang, H. Zhi, Z. Wang, and L. Feng (2015), ENSO modulations due to interannual variability of freshwater forcing and ocean biology-induced heating in the tropical Pacific, *Sci. Rep.*, *5*, 18506, doi:10.1038/srep18506.

Zhu, J., G.-Q. Zhou, R.-H. Zhang, and Z. Sun (2011), On the role of oceanic entrainment temperature (Te) in decadal changes of El Niño/Southern Oscillation, *Ann. Geophys.*, *29*, 529–540, doi:10.5194/angeo-29-529-2011.

Zhu, J., B. Huang, L. Marx, J. L. Kinter III, M. A. Balmaseda, R.-H. Zhang, and Z.-Z. Hu (2012), Ensemble ENSO hindcasts initialized from multiple ocean analyses, *Geophys. Res. Lett.*, *39*, L09602, doi:10.1029/2012GL051503.

Zhu, J., G.-Q. Zhou, R.-H. Zhang, and Z. Sun (2013a), Improving ENSO prediction in a hybrid coupled model with an embedded entrainment temperature parameterization, *Int. J. Climatol.*, *33*, 343–355, doi:10.1002/joc.3426.

Zhu, J., B. Huang, M. A. Balmaseda, J. L. Kinter III, P. Peng, Z.-Z. Hu, and L. Marx (2013b), Improved reliability of ENSO hindcasts with multi-ocean analyses ensemble initialization, *Clim. Dyn.*, *41*, 2785–2795, doi:10.1007/s00382-013-1965-8.

Zhu, J., et al. (2015), ENSO prediction in project Minerva: Sensitivity to atmospheric horizontal resolution and ensemble size, *J. Clim.*, *28*, 2080–2095, doi:10.1175/JCLI-D-14-00302.1.

Zhu, J., W. Wang, and A. Kumar (2017a), Simulations of MJO propagation across the Maritime Continent: Impacts of SST feedback, *J. Clim.*, *30*, 1689–1704, doi:10.1175/JCLI-D-16-0367.1.

Zhu, J., A. Kumar, H.-C. Lee, and H. Wang (2017b), Seasonal predictions using a simple ocean initialization scheme, *Clim. Dyn.*, doi:10.1007/s00382-017-3556-6.